第 46 卷 第 6 期
2017 年 11 月

地球化学
GEOCHIMICA

Vol.46, No.6, 497~510
Nov., 2017

冈底斯带南部新特提斯洋早期俯冲有关岩浆特征与成矿分析

邹银桥[1,2], 陈喜连[1,2], 黄文婷[1], 张 健[1,2],
梁华英[1*], 许继峰[3], 陈 玲[4]

(1. 中国科学院 广州地球化学研究所 中国科学院矿物学与成矿学重点实验室, 广东 广州 510640; 2. 中国科学院大学, 北京 100049; 3. 中国科学院 广州地球化学研究所 同位素地球化学国家重点实验室, 广东 广州 510640; 4. 钦州学院 广西北部湾海洋灾害研究重点实验室, 广西 钦州 535011)

摘 要: 冈底斯南缘经历了新特提斯洋俯冲及其后的陆陆碰撞, 发育众多后碰撞环境的斑岩铜矿床, 而与洋壳俯冲有关斑岩型矿床却发现不多, 目前仅有雄村斑岩型铜金矿床。本工作在冈底斯南缘东西向 200 多千米范围内发现多个铜矿化岩体及火山岩。岩体锆石 U-Pb 年龄显示其侵位于早中侏罗世。这些铜矿化岩体及火山岩多发育脉状帘石化蚀变, 而其周围新生代岩基多未发生蚀变及矿化, 显示矿化及蚀变早于新生代岩基; 而磁铁矿-赤铁矿-黄铜矿矿物组合表明铜矿化与岩浆磁铁矿的氧化还原过程有关, 矿化时代与岩体基本同期。矿化岩体多富含角闪石, 发育磁铁矿-赤铁矿组合, 显示岩浆富水氧化特征, 而岩浆期榍石、磷灰石及石英中发育原生流体包裹体, 显示富水岩浆较早出溶挥发分。综合区内早中生代岩浆岩的时空分布, 冈底斯南缘存在东西向的侏罗纪弧岩浆岩带。该套岩浆岩具有典型弧岩浆地球化学特征, 锆石$\varepsilon_{Hf}(t)$值(+10 ~ +16)显示近亏损地幔端元的源区特征。上述证据表明, 冈底斯南缘在早中生代发生了大范围的岩浆活动和同期铜矿化, 新生下地壳或亏损地幔源区可提供良好的 Cu 金属来源, 高氧化富水的母岩浆有利于亲铜元素的富集与成矿, 为斑岩铜矿床形成的有利条件。据此, 我们提出冈底斯南缘在早中侏罗世可能存在一个包括雄村斑岩型铜金矿床在内的高氧化岩浆岩和矿化带, 其与新特提斯洋洋壳在侏罗纪俯冲引发的大规模的岩浆活动相关, 该带具备良好的斑岩铜矿找矿前景。鉴于冈底斯南缘在白垩纪之后经历了大规模抬升和剥蚀, 在该地区寻找新的俯冲型斑岩铜金矿床应主要集中在早中侏罗世火山岩出露区。

关键词: 冈底斯南缘; 早中生代岩浆岩; 富水高氧化岩浆带; 斑岩型铜矿床

中图分类号: P597; P612; P618.41 文献标识码: A 文章编号: 0379-1726(2017)06-0497-14

Magmatic properties and metallogenic analyses of magmatism triggered by early Neo-Tethys subduction in South Gangdese, Tibet

ZOU Yin-qiao[1,2], CHEN Xi-lian[1,2], HUANG Wen-ting[1], ZHANG Jian[1,2],
LIANG Hua-ying[1*], XU Ji-feng[3] and CHEN Ling[4]

1. *Key Laboratory of Mineralogy and Metallogeny, Guangzhou Institute of Geochemistry, Chinese Academy of Sciences, Guangzhou* 510640, *China*;
2. *University of Chinese Academy of Sciences, Beijing* 100049, *China*;
3. *State Key Laboratory of Isotope Geochemistry, Guangzhou Institute of Geochemistry, Chinese Academy of sciences, Guangzhou* 510640, *China*;
4. *Guangxi Key Laboratory of Marine Disaster in the Beibu Gulf, Qinzhou University, Guangxi, Qinzhou* 535011, *China*

Abstract: South Gangdese has experienced the Neo-Tethys subduction and subsequent collision between the Indian and Eurasian plates. Many post-collision-related porphyry Cu-Mo deposits have been found in the South Gangdese belt. However, only the Xiongcun super-large porphyry Cu-Au deposit was identified as relating to the Neo-Tethys subduction in the South Gangdese belt. This work reports several Cu-mineralized intrusions in the

收稿日期**(Received):** 2016-10-27; 改回日期**(Revised):** 2017-03-22; 接受日期**(Accepted):** 2017-04-12
基金项目: 中国科学院战略性先导科技专项(B 类) (XDB03010302); 科技部国家重点研究计划(2016YFC0600407)
作者简介: 邹银桥(1991–), 男, 博士研究生, 矿物学岩石学矿床学专业。E-mail: 554604088@qq.com
* 通讯作者**(Corresponding author):** LIANG Hua-ying, E-mail: lianghy@gig.ac.cn, Tel: +86-20-85290107

South Gangdese belt, which are distributed widely from the west to the east. Zircon U-Pb ages show that they were emplaced in the Early Mesozoic. Such Cu-mineralized igneous rocks generally develop quartz-epidote vein alterations, while the surrounding Cretaceous-Cenozoic Gangdese granitic batholith did not undergo any corresponding alteration and mineralization. This finding suggests that Cu mineralization and alteration occurred earlier than the batholith's formation. The chalcopyrite-magnetite-hematite mineral assemblage shows that Cu mineralization was related to the redox process of the magmatic magnetite. Thus, the mineralization was coeval with the intrusions. These Jurassic rocks have high hornblende content and quartz-magnetite-titanite and hematite-magnetite mineral assemblages, indicating they originated from highly oxidized and water-rich magmas. The primary fluid inclusions found in the magmatic sphere and apatite of mineralized intrusions indicate that their parental water-rich magmas existed in an exsolved volatile phase during the early stage of the magma evolution process. The temporal and spatial distributions of the Early Mesozoic magmatic rocks show the existence of a west-east magmatic rock belt parallel to the Yarlung Zangbo suture zone in the South Gangdese. These Early Mesozoic magmatic rocks show typical arc magma characteristics, and have high positive zircon $\varepsilon_{Hf}(t)$ (+10 ~ +16), providing evidence of a mantle-derived magma source. The above findings imply that South Gangdese developed large-scale magmatism associated with Cu mineralization in the Early Mesozoic. These Jurassic magmatic rocks originated from a juvenile lower crust, which provided a good Cu metal source. Further, their parental magmas were highly oxidized water-rich magmas, favoring the concentration and mineralization of chalcophile elements during the magma evolution process. Thus, it is proposed that the Early-Middle Jurassic subduction of the Neo-Tethys slab induced a west-east oxidized arc magmatic rock belt and contemporary Cu mineralization in the South Gangdese belt. The results reveal there was good potential for the creation of subduction-related porphyry Cu deposits. Given the strong uplift and denudation in South Gangdese after the Cretaceous, the domains of the Early-Middle Jurassic volcanic rocks or intrusions associated with Cu mineralization in this area are a good prospecting target for subduction-related porphyry Cu deposits.

Key words: South Gangdese; Early-Middle Jurassic igneous rocks; water-rich and oxidized magma; porphyry Cu deposit

0 引 言

冈底斯南缘位于雅鲁藏布江缝合带北侧，经历了新特提斯洋俯冲及其后的陆陆碰撞[1−2]。目前在该带上发现了一系列新生代碰撞环境下的斑岩铜钼矿床，形成我国重要的斑岩铜钼矿带[3−10]。区内与大洋板块俯冲相关的斑岩型矿床却极少，目前仅在谢通门县发现形成于早中侏罗世的雄村特大斑岩型铜金矿床[11−13]。世界上斑岩矿床多和俯冲构造岩浆活动有关，但冈底斯南缘俯冲型斑岩矿床却发现较少。造成这一现象的主要原因是什么？是冈底斯南缘俯冲环境形成的岩浆不利于成矿？还是早中侏罗世形成的斑岩型矿床在新生代大规模抬升过程中被剥蚀？为了分析这些问题，很有必要分析冈底斯南缘早中侏罗世岩浆活动规模、特征及其是否有利于成矿元素在岩浆形成演化过程中富集成矿。

本工作在冈底斯南缘桑日群火山岩出露地区发现多个铜矿化岩体，分析矿化岩体锆石 U-Pb 年龄及岩浆富水高氧化特征。该工作对评价冈底斯南缘俯冲型斑岩铜矿床的成矿潜力具有重要意义。

1 区域地质背景

拉萨地块位于雅鲁藏布江缝合带和班公湖-怒江缝合带之间(图 1a)。自中生代以来，拉萨地块南部先后经历了新特提斯雅鲁藏布江洋壳俯冲和其后的弧-陆碰撞、陆-陆碰撞造山作用，形成一系列与洋壳俯冲及陆陆碰撞有关的火山岩和侵入岩。目前较多地质、地球物理及地球化学证据表明，新特提斯洋自早中生代开始俯冲，直至 65~50 Ma 印度板块与欧亚板块在发生碰撞[1,21,22]。

冈底斯带为拉萨地块内的巨型构造-岩浆岩带，东西长约 2500 km，南北宽 150~300 km，面积达

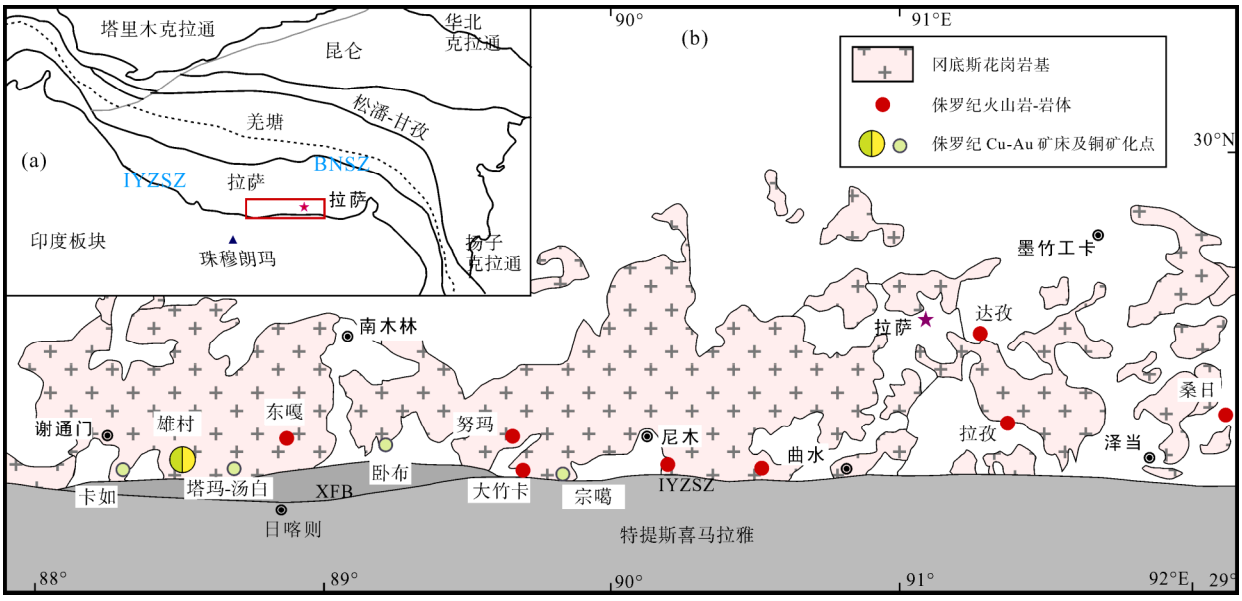

图 1　冈底斯南缘岩浆岩分布简图(据文献[12]修改)

Fig.1　Sketch map showing the distribution of igneous rocks in South Gangdese (modified after [12])

(a)为青藏高原大地构造简图; 浅绿标志为本工作发现的矿化岩体, 红色标志为侏罗纪岩体(据文献[11,14–20])。

BNSZ–班公湖怒江缝合带; IYZSZ–雅鲁藏布江缝合带; XFB–日喀则弧前盆地。

(a) Tectonic sketch of the Tibet plateau. Intrusions denoted by the light green and red circles are from our work and previous work[11,14–20], respectively. Abbreviations: BNSZ– Bangong-Nujiang suture zone; IYZSZ– Indus Yarlung Zangbo suture zone; XFB– Xigazeforearc basin.

45 万 km^2[23]。冈底斯带岩浆岩主要形成于新生代[24–25], 少量形成于晚中生代。其中新生代岩浆岩包括 53~47 Ma 的冈底斯花岗岩[26]、65~41 Ma 的林子宗火山岩[27], 少量中新世岩浆岩主要为钾质-超钾质火山岩及钾质二长花岗斑岩。白垩纪桑日群火山岩[28–29]及中酸性侵入岩在冈底斯带分布较为广泛, 为新特提斯洋俯冲引发的弧岩浆产物产物[30–32]。侏罗纪叶巴组火山岩主要分布在达孜–工布江达一带[33–34], 同期侵入体在冈底斯带中西部有零星出露, 普遍与上部同期火山岩共生, 岩性主要为花岗岩、二长花岗岩、花岗闪长岩及闪长(斑)岩, 局部见少量的辉长岩[35]。

冈底斯带南缘发育两类不同元素组合的斑岩型矿床, 一为斑岩型铜钼矿床, 另一为斑岩型铜金矿床。前者规模大, 构成东西向斑岩铜钼成矿带, 形成时代主要集中于 18~13 Ma, 与碰撞后环境中酸性岩浆活动有关[3–10]; 后者目前发现较少, 仅发现有雄村特大斑岩型铜金矿床, 成矿元素以 Cu-Au 为主, 形成于中侏罗世(160~180 Ma)[11–12]。

2　矿化岩体特征

本次研究在冈底斯南缘从谢通门向东约 250 km 长的剖面上作了系统野外调查, 在卡如、塔玛、洞嘎、卧布、宗嘎等地发现火山岩及其共生的中酸性侵入岩(图 1b)。该套火山岩及共生的侵入岩多见铜矿化及石英-绿帘石细脉状蚀变, 而其周围的白垩世-新生代的冈底斯花岗岩基则未见有关矿化及蚀变(图 2)。

卡如岩体位于谢通门县往东约 10 km 处(图 1b), 上部主要被第四纪坡积物及少量火山沉积岩覆盖(图 3a), 在多条冲刷较深的沟中及公路旁可见新鲜岩体露头。岩体普遍发育脉状石英-绿帘石化蚀变, 局部见孔雀石化(图 3b)。矿化岩体外围为白垩纪钾长石黑云母石英闪长岩, 与卡如岩体侵入接触(图 2a)。白垩纪黑云母石英闪长岩未见蚀变及矿化。镜下特征显示, 卡如岩体为花岗结构, 块状构造。主要矿物含石英 20%~25%, 斜长石 60%~65%, 角闪石约为 8%~12%; 钾长石含量较少(2%~4%); 副矿物中榍石与磁铁矿较为发育, 常见磷灰石等(图 4a), 定名为花岗岩。斜长石部分绢云母化, 角闪石多已绿帘石化, 但保持双晶形态(图 4a)。

塔玛岩体出露于谢通门县至日喀则公路检查站附近(图 1b), 位于桑日群比马组火山岩出露区。在公路旁以及冲刷较深的沟中能看到新鲜岩体露头。野外产状表明, 岩体产于桑日群火山岩底部, 与上部火山岩侵入接触(图 3c)。岩体与火山岩内均发育较

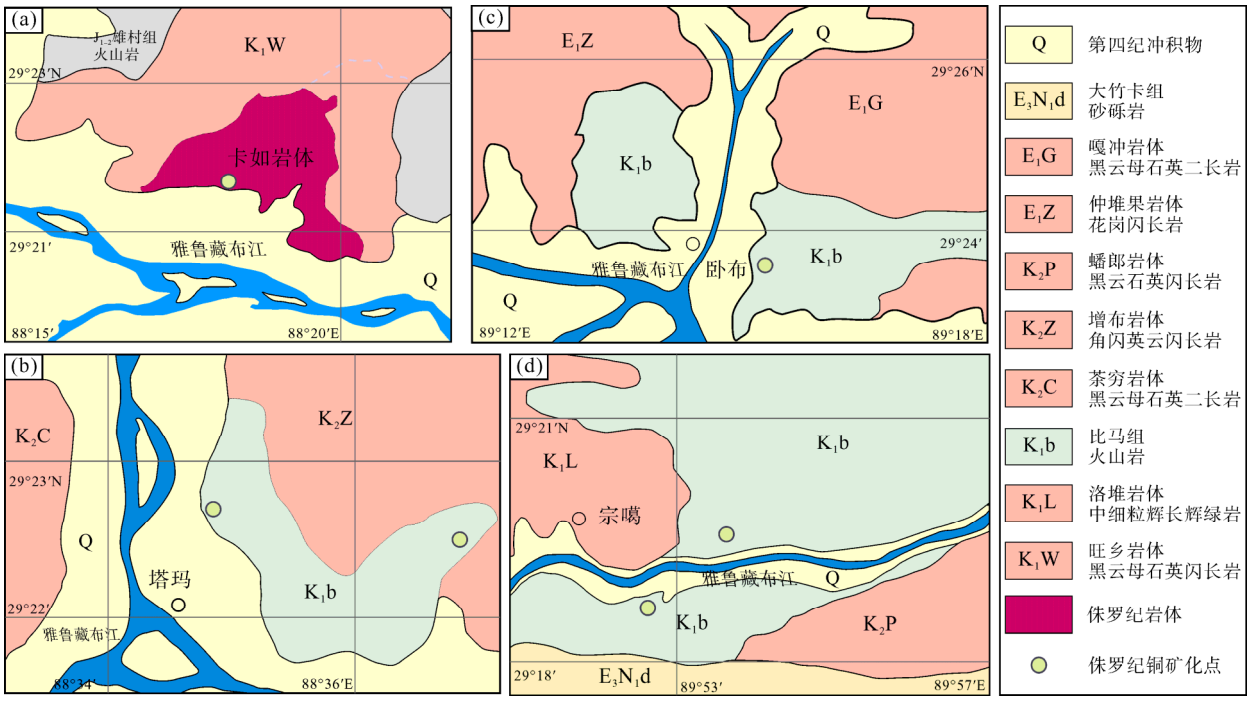

图 2　矿化岩体区域地质简图(据 1∶25 万区域地质图)

Fig.2　Simple geological maps of the mineralized magmatic rocks (after the regional geological map of scale 1∶250, 000)

(a) 卡如岩体; (b) 塔玛岩体; (c) 卧布岩体; (d) 宗噶岩体。

强的脉状石英-绿泥石化蚀变(图 3d)，多处见 Cu 的次生氧化及褐铁矿化。外围的晚白垩中粗粒黑云母二长闪长岩，与塔玛岩体及桑日群火山岩侵入接触，岩石未见蚀变与矿化(图 2b)。塔玛岩体蚀变较强，主要矿物为石英 18%~25%，斜长石 60%~65%，角闪石(绿帘石化)15%~20%；副矿物见磷灰石、磁铁矿等，定名为绿帘石化花岗岩。角闪石多已蚀变为绿帘石，斜长均发生石绢云母化(图 4b)。

卧布岩体出露于日喀则地区艾玛乡附近(图 1b)，区域上大面积出露桑日群比马组火山岩，仅在采石场及冲刷较深沟中局部见新鲜岩体露头。野外产状表明，卧布岩体与上部比马组火山岩沉积岩、火山角砾岩及安山岩侵入接触(图 3e)，岩体内外普遍发育绿帘石化蚀变，局部见孔雀石化(图 3f)。岩体外围为新生代古近纪花岗岩基(图 2c)，与矿化岩体侵入接触，且未见矿化蚀变，显示为矿化后岩体。卧布岩体斑状结构，斑晶含量约为 15%~20%，主要为角闪石 15%左右、斜长石与石英占 5%左右；基质为石英 15%~20%、斜长石(基本蚀变成绢云母)45%~50%和钾长石 5%~8%，定名闪长斑岩(图 4c)。角闪石具暗化边结构，基本已蚀变为绿帘石-绿泥石等矿物。

宗噶岩体位于日喀则吉隆县宗噶乡雅鲁藏布江北侧，区域内大面积出露比马组安山岩-火山凝灰岩(图 2d 和 3g)，公路边及采石场可见新鲜岩体露头。岩体野外产状表明，宗噶岩体上部发育较厚风化层，与顶部桑日群火山岩不整合接触(图 3g)。岩体内发育脉状绿帘石化蚀变，局部见孔雀石矿化(图 3h)。桑日群火山岩外围为早白垩世黑云母石英闪长岩和辉长岩体，为冈底斯岩基一部分，新鲜无矿化蚀变。宗噶岩体为花岗结构，主要矿物为石英 20%~25%，斜长石 60%~65%，角闪石 12%~15%以及少量钾长石 5%左右；副矿物见磁铁矿、磷灰石与锆石，定名为花岗岩(图 4d)。斜长石多发于绢云母化，角闪石部分蚀变为绿帘石。

3　分析方法

本文对塔玛绿帘石化花岗岩与宗噶花岗岩进行了锆石 LA-ICP-MS U-Pb 同位素定年分析。将两个样品粉碎至 60 目，经水淘、磁选后，在双目镜下挑选出自形的晶型较好的锆石。将待测锆石置于环氧树脂中制成靶、打磨至锆石中心部位暴露并抛光。利用阴极发光(CL)扫描电镜进行图像分析确定单颗粒锆石的形态、结构。结合光学显微镜观察，以选择颗粒大、较自形清晰无裂纹、无包体的锆石用于分析。

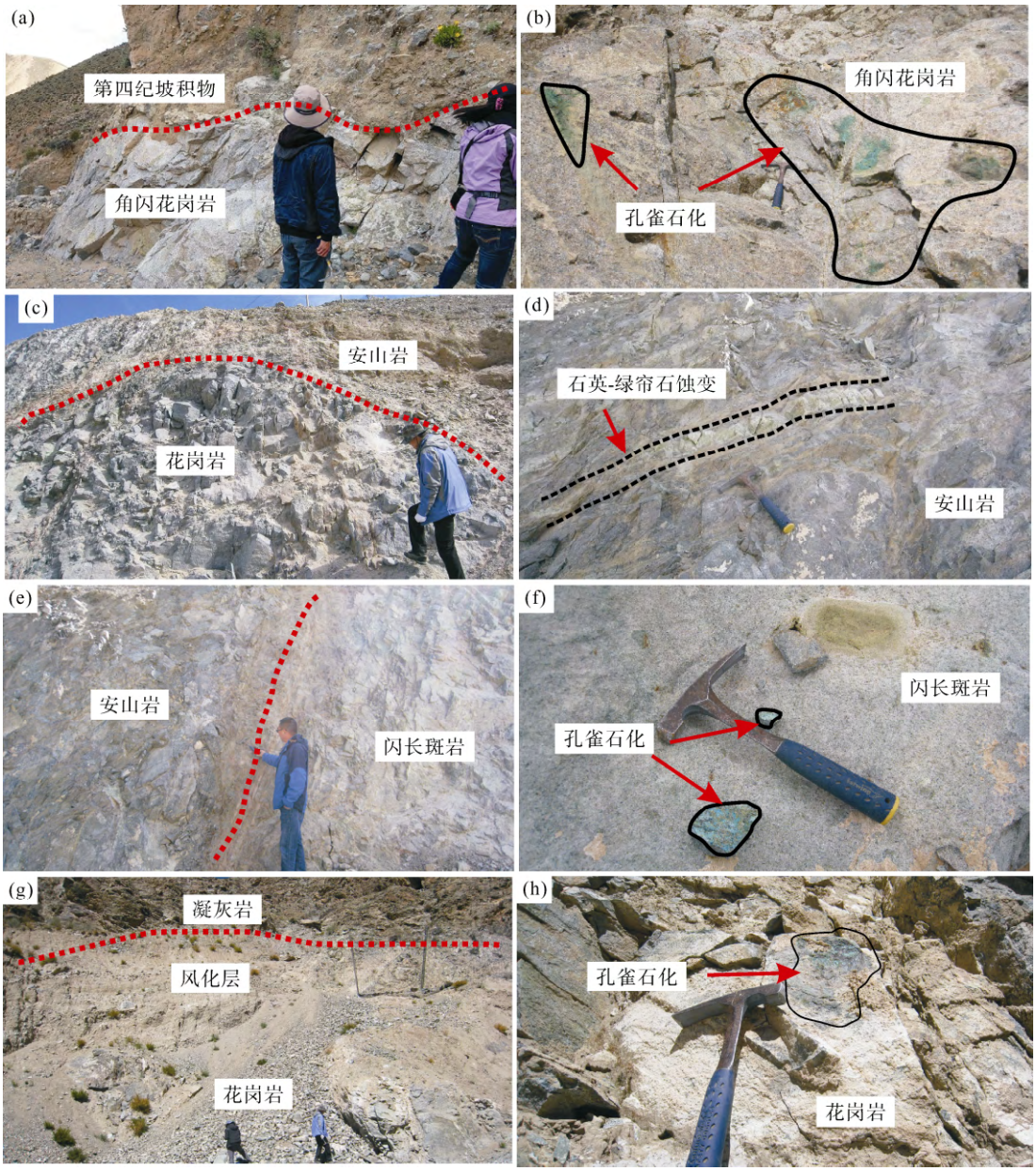

图 3　冈底斯南缘蚀变矿化火山岩-岩体野外产状

Fig.3　Field photographs of the mineralized volcanic rocks and intrusions in South Gangdese

(a) 卡如角闪花岗岩上部为坡积物; (b) 卡如角闪花岗岩内局部见孔雀石化; (c) 塔玛花岗岩及上部安山岩; (d) 塔玛安山岩中石英-绿帘石脉; (e) 卧布闪长斑岩与安山岩; (f) 卧布闪长斑岩局部孔雀石化; (g) 宗噶花岗岩及上部凝灰岩; (h) 宗噶花岗岩中的铜矿化。

锆石原位微区 LA-ICP-MS U-Pb 定年及锆石微量元素分析在西北大学大陆动力学国家重点实验室完成。使用标准锆石 91500 和 GJ-1 作年龄标样，微量元素采用 NIST 610 标样校正。用 ICPMSDataCal 7.2 软件对分析数据进行计算，锆石的 U-Pb 年龄谐和图绘制和年龄加权平均年龄计算采用 ISOPLOT。

4　岩体时代及矿化与岩体的关系分析

塔玛岩体和宗噶岩体的锆石颗粒均较自形，呈短柱状-柱状，发育清晰的振荡环带结构(图 5)。锆石 Th/U 比值都较高，在 0.47~0.93 之间(表 1)，显示了岩浆锆石的特征。

锆石 LA-ICP-MS U-Pb 年龄结果见表 1。塔玛绿帘石化花岗岩共进行了 25 个锆石分析点，删除其中 6 个谐和度较低的数据。2 个继承锆石点以及 2 个 Pb 丢失锆石数据点不加入计算，其余主群锆石加权平均年龄为(185.3±2.0) Ma, MSWD = 0.99 (图 6a)。宗噶花岗岩 25 个锆石分析点数据 $^{206}Pb/^{238}U$ 年龄较

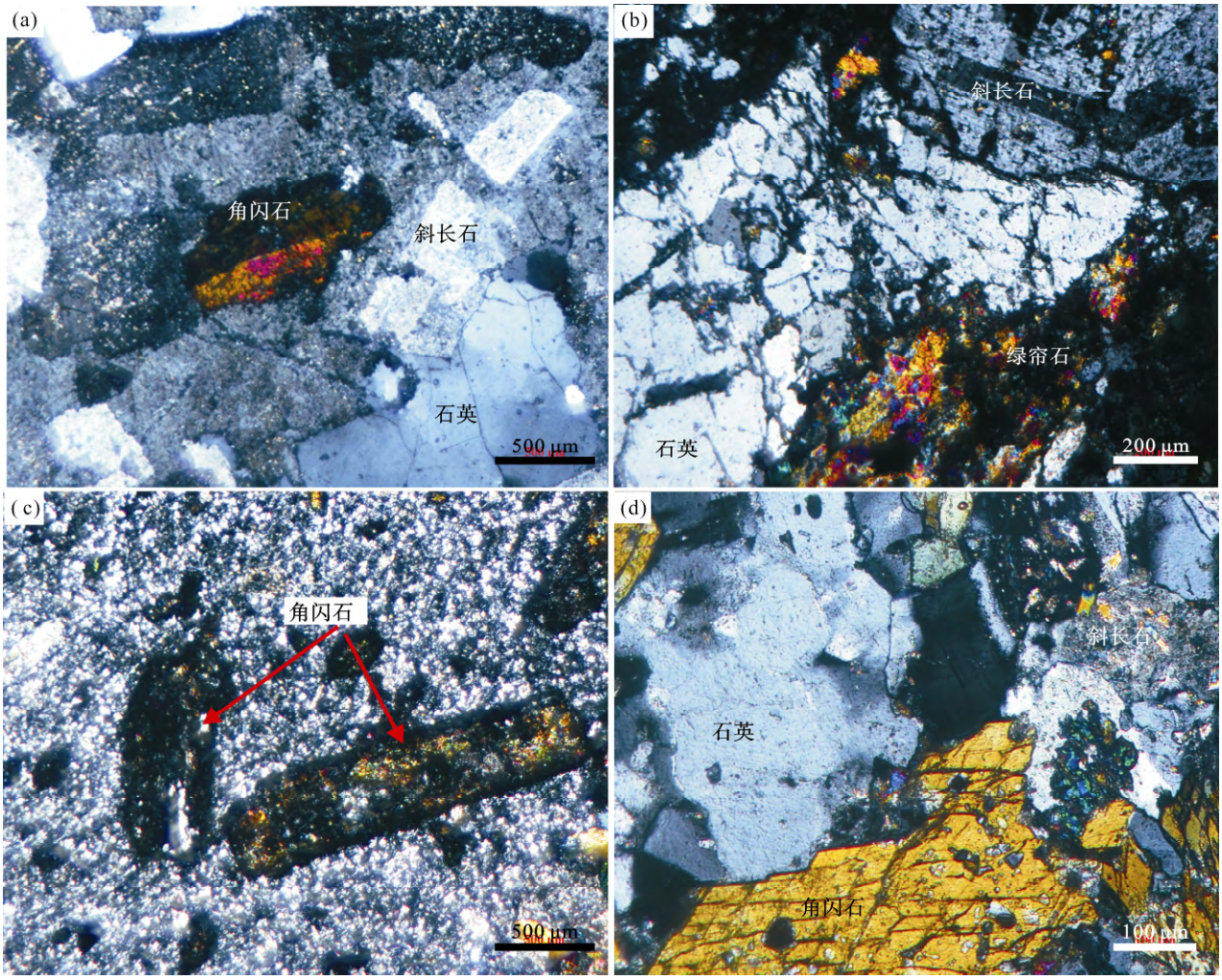

图 4　矿化岩体显微照片

Fig.4　Micrographs of the mineralized intrusions.

(a) 卡如岩体; (b) 塔玛岩体; (c) 卧布岩体; (d) 宗噶岩体。

为集中，在 231~244 Ma 之间, 25 颗主群锆石加权平均年龄为(237.3±1.3) Ma, MSWD = 1.7 (图 6b)。

年代学研究表明，塔玛岩体与宗噶岩体年龄分别为(185.3±2.0) Ma 和(237.3±1.3) Ma (MSWD = 2.7) (图 6)，都形成于早中生代。另外，卡如、卧布岩体被证实分别侵位于(177.3±3.2) Ma 和(166.3±1.3) Ma，塔玛岩体上覆比马组火山岩时代为(180.2±0.8) Ma (年龄数据已在另文发表)。上述年龄数据表明，矿化岩体形成于晚三叠世至早侏罗世。

野外观察表明，脉状石英-绿帘石化蚀变及铜矿化仅发育在中生代岩体及火山岩内，其周围的冈底斯花岗岩基则未见蚀变及矿化，说明铜矿化及蚀变作用应早于冈底斯花岗岩基；目前冈底斯南缘中生代以来主要经历了和俯冲岩浆作用及碰撞岩浆作用有关的两期铜矿化，该矿化早于与碰撞作用有关的岩基，因此，矿化时代应和赋矿岩体有关。

在卧布铜矿化闪长斑岩中，发育黄铜矿-磁铁矿-赤铁矿共生组合(图 7b)。岩体中原生的磁铁矿-赤铁矿组合多为高氧化岩浆演化晚期的产物[36]，而岩浆演化晚期至成矿早期，氧化硫和亚铁反应，形成磁铁矿。同时氧化硫被还原，还原硫和铜及亚铁结合形成黄铜矿，因而会形成磁铁矿-赤铁矿-黄铜矿组合[36]。这一矿物组合表明卧布闪长斑岩中铜矿化是岩浆演化至晚期的产物，矿化时代与岩体侵位时代基本一致，铜矿化和岩体有内在成因联系。这些矿化岩体形成时代与冈底斯南缘雄村斑岩型铜金矿床成岩成矿时代相近[11]，位于同一构造岩浆带，都和新特提斯洋俯冲有关。

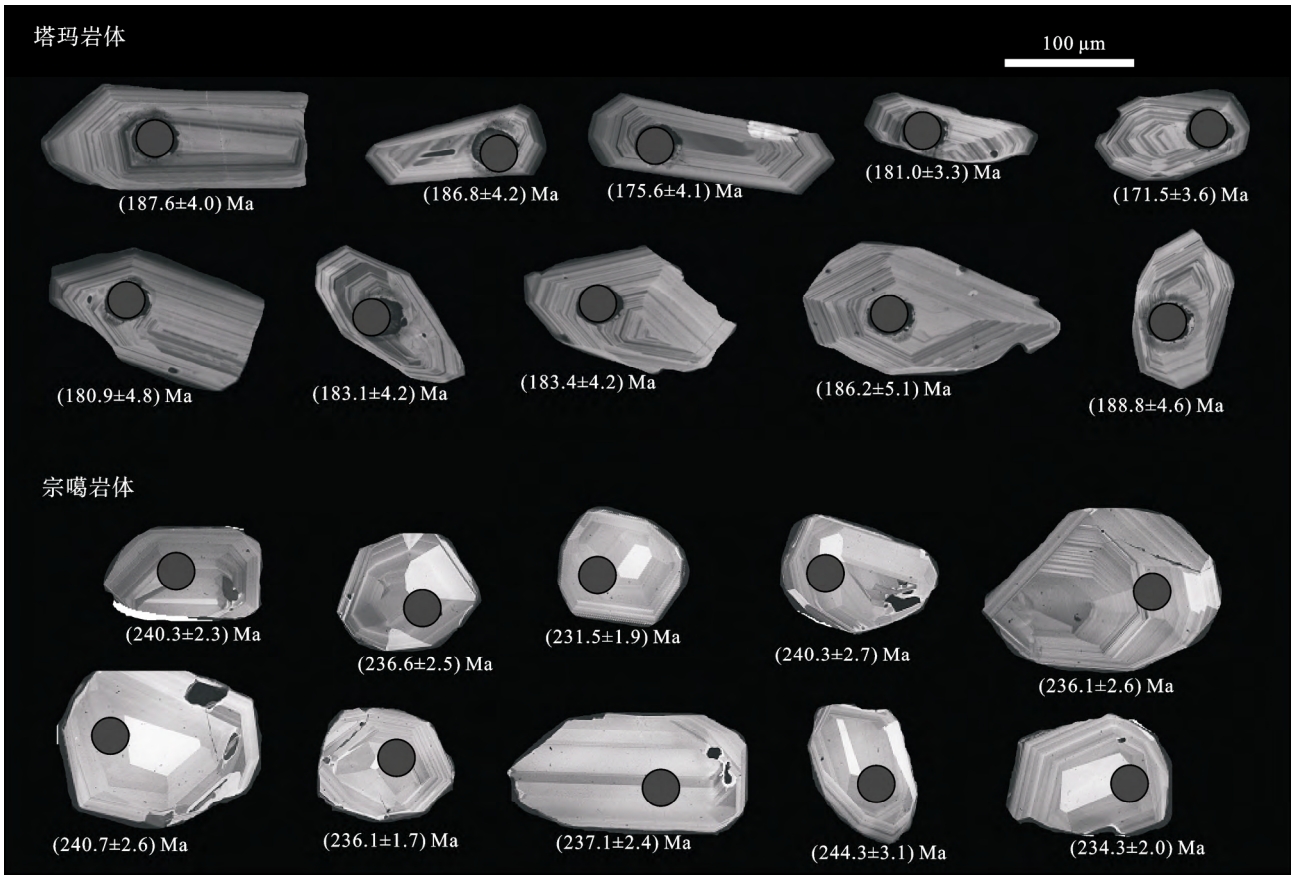

图 5　塔玛岩体与宗噶岩体的锆石阴极发光(CL)图像

Fig.5　Cathodoluminescence (CL) images of representative zircon grains of the Tama and Zongga intrusions

表 1　塔玛岩体与宗噶岩体 **LA-ICP-MS** 锆石 **U-Pb** 同位素分析数据表

Table 1　Zircon U-Pb isotope data of the Tama and Zongga intrusions

分析号	Th/U	$^{207}Pb/^{206}Pb$	±1σ	$^{207}Pb/^{235}U$	±1σ	$^{206}Pb/^{238}U$	±1σ	$^{207}Pb/^{235}U$ 年龄(Ma)	±1s.e.	$^{206}Pb/^{238}U$ 年龄(Ma)	±1σ	谐和度
塔玛岩体												
XC-15-1	0.5	0.05152	0.00329	0.21890	0.01388	0.03099	0.00065	201.0	11.6	166.9	4.1	97%
XC-15-2	0.5	0.05329	0.00359	0.20692	0.01393	0.02847	0.00064	191.0	11.7	187.6	4.0	94%
XC-15-3	0.4	0.07104	0.00590	0.28112	0.02282	0.02941	0.00068	251.5	18.1	186.8	4.2	70%
XC-15-4	0.4	0.05148	0.00406	0.20515	0.01606	0.02898	0.00057	189.5	13.5	191.2	3.6	97%
XC-15-5	0.5	0.05711	0.00466	0.21315	0.01723	0.02761	0.00066	196.2	14.4	175.6	4.1	88%
XC-15-6	0.7	0.04227	0.00277	0.16355	0.01029	0.02847	0.00053	153.8	9.0	181.0	3.3	83%
XC-15-7	0.7	0.06418	0.00346	0.22905	0.01265	0.02595	0.00051	209.4	10.4	165.1	3.2	76%
XC-15-8	0.5	0.05314	0.00300	0.21505	0.01215	0.02971	0.00060	197.8	10.2	196.8	3.8	95%
XC-15-9	0.4	0.05781	0.00458	0.22524	0.01622	0.02938	0.00075	206.3	13.4	209.2	4.7	90%
XC-15-10	0.5	0.04684	0.00339	0.18688	0.01428	0.02886	0.00057	174.0	12.2	171.5	3.6	94%
XC-15-11	0.5	0.05702	0.00400	0.22940	0.01578	0.03011	0.00067	209.7	13.0	179.8	4.2	90%
XC-15-12	0.9	0.04921	0.00249	0.17886	0.00913	0.02623	0.00036	167.1	7.9	179.9	2.2	99%
XC-15-13	0.5	0.05050	0.00393	0.22682	0.01818	0.03299	0.00077	207.6	15.0	180.9	4.8	99%
XC-15-14	0.4	0.04974	0.00397	0.19597	0.01531	0.02884	0.00068	181.7	13.0	183.1	4.2	99%
XC-15-15	0.5	0.04811	0.00362	0.19859	0.01518	0.03002	0.00069	183.9	12.9	183.3	4.3	96%
XC-15-16	0.5	0.05225	0.00441	0.20340	0.01579	0.02881	0.00067	188.0	13.3	183.4	4.2	97%
XC-15-17	0.6	0.05113	0.00403	0.20743	0.01679	0.02953	0.00075	191.4	14.1	184.2	4.7	98%
XC-15-18	0.4	0.05752	0.00502	0.22350	0.01851	0.02931	0.00082	204.8	15.4	186.2	5.1	90%
XC-15-19	0.6	0.05176	0.00384	0.19079	0.01342	0.02695	0.00050	177.3	11.4	186.6	3.1	96%

(续表 1)

分析号	Th/U	$^{207}Pb/^{206}Pb$	±1σ	$^{207}Pb/^{235}U$	±1σ	$^{206}Pb/^{238}U$	±1σ	$^{207}Pb/^{235}U$ 年龄(Ma)	±1s.e.	$^{206}Pb/^{238}U$ 年龄(Ma)	±1σ	谐和度
塔玛岩体												
XC-15-20	0.5	0.05252	0.00367	0.21228	0.01414	0.02990	0.00074	195.5	11.8	188.8	4.6	97%
XC-15-21	0.5	0.05258	0.00348	0.19939	0.01297	0.02828	0.00066	184.6	11.0	189.6	4.1	97%
XC-15-22	0.7	0.05245	0.00281	0.20557	0.01085	0.02830	0.00050	189.8	9.1	189.9	3.1	94%
XC-15-23	0.6	0.06033	0.00374	0.22213	0.01287	0.02709	0.00055	203.7	10.7	172.3	3.5	83%
XC-15-24	0.5	0.06804	0.00575	0.24823	0.02208	0.02893	0.00087	225.1	18.0	183.8	5.4	79%
XC-15-25	0.7	0.05381	0.00291	0.21861	0.01210	0.02985	0.00060	200.8	10.1	190.7	3.8	94%
宗噶岩体												
15XC-52-01	1.3	0.05270	0.00128	0.27584	0.00661	0.03799	0.00037	247.4	5.3	240.3	2.3	97%
15XC-52-02	1.1	0.05144	0.00114	0.26618	0.00667	0.03738	0.00041	239.6	5.3	236.6	2.5	98%
15XC-52-03	1.1	0.05243	0.00153	0.27560	0.00860	0.03805	0.00041	247.2	6.8	240.7	2.6	97%
15XC-52-04	0.9	0.05520	0.00149	0.28464	0.00738	0.03754	0.00039	254.3	5.8	237.5	2.4	93%
15XC-52-05	1.6	0.05134	0.00084	0.26458	0.00452	0.03731	0.00028	238.3	3.6	236.1	1.7	99%
15XC-52-06	1.1	0.05690	0.00152	0.29611	0.00902	0.03746	0.00039	263.4	7.1	237.1	2.4	89%
15XC-52-07	0.8	0.05239	0.00124	0.27142	0.00660	0.03756	0.00038	243.8	5.3	237.7	2.4	97%
15XC-52-08	1.4	0.05099	0.00112	0.25712	0.00561	0.03657	0.00030	232.3	4.5	231.5	1.9	99%
15XC-52-09	0.7	0.05184	0.00138	0.27101	0.00721	0.03798	0.00043	243.5	5.8	240.3	2.7	98%
15XC-52-10	0.7	0.05090	0.00146	0.27056	0.00804	0.03862	0.00050	243.1	6.4	244.3	3.1	99%
15XC-52-11	0.9	0.05155	0.00154	0.26467	0.00782	0.03730	0.00041	238.4	6.3	236.1	2.6	99%
15XC-52-12	0.8	0.04981	0.00095	0.25480	0.00510	0.03702	0.00033	230.5	4.1	234.3	2.0	98%
15XC-52-13	0.7	0.05439	0.00200	0.28935	0.01190	0.03833	0.00053	258.0	9.4	242.5	3.3	93%
15XC-52-14	1.1	0.04978	0.00092	0.25956	0.00525	0.03777	0.00038	234.3	4.2	239.0	2.3	98%
15XC-52-15	1.4	0.05272	0.00113	0.27034	0.00599	0.03729	0.00048	243.0	4.8	236.0	3.0	97%
15XC-52-16	0.8	0.04866	0.00099	0.24942	0.00555	0.03709	0.00037	226.1	4.5	234.8	2.3	96%
15XC-52-17	0.8	0.05080	0.00114	0.26439	0.00653	0.03773	0.00050	238.2	5.2	238.7	3.1	99%
15XC-52-18	1.1	0.05084	0.00096	0.25877	0.00550	0.03684	0.00033	233.7	4.4	233.2	2.1	99%
15XC-52-19	0.9	0.04958	0.00150	0.25875	0.00795	0.03796	0.00043	233.7	6.4	240.2	2.6	97%
15XC-52-20	0.8	0.05111	0.00137	0.26886	0.00752	0.03824	0.00050	241.8	6.0	241.9	3.1	99%
15XC-52-21	0.8	0.05019	0.00143	0.26260	0.00755	0.03806	0.00044	236.8	6.1	240.8	2.7	98%
15XC-52-22	1.3	0.05226	0.00124	0.26914	0.00656	0.03734	0.00029	242.0	5.2	236.3	1.8	97%
15XC-52-23	0.7	0.05049	0.00149	0.26851	0.00846	0.03861	0.00056	241.5	6.8	244.2	3.5	98%
15XC-52-24	0.8	0.05061	0.00118	0.25997	0.00630	0.03729	0.00037	234.6	5.1	236.0	2.3	99%
15XC-52-25	0.9	0.05010	0.00128	0.25838	0.00625	0.03755	0.00035	233.4	5.0	237.6	2.2	98%

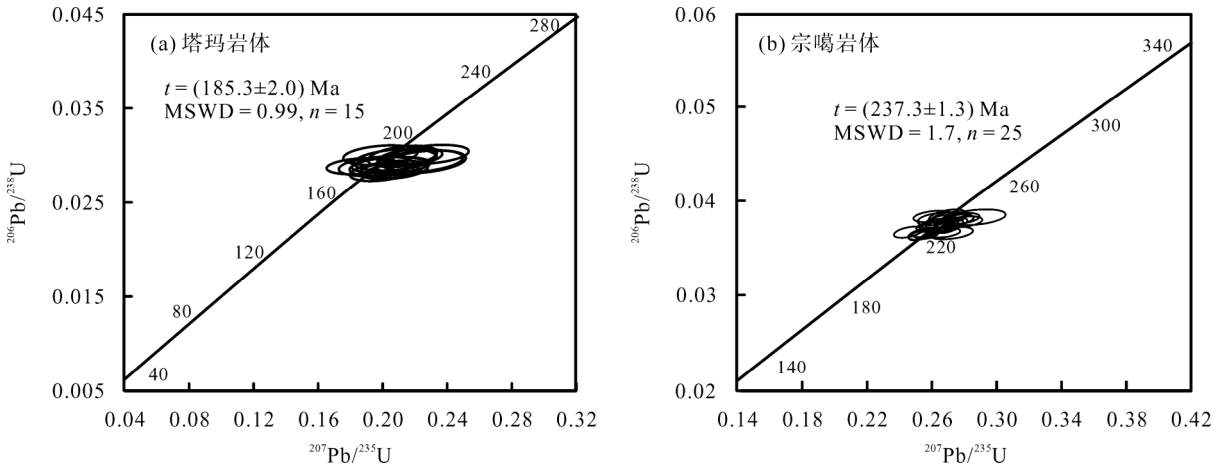

图 6 铜矿化岩体的锆石 U-Pb 年龄谐和图

Fig.6 Zircon U-Pb concordia diagrams of the mineralized intrusions

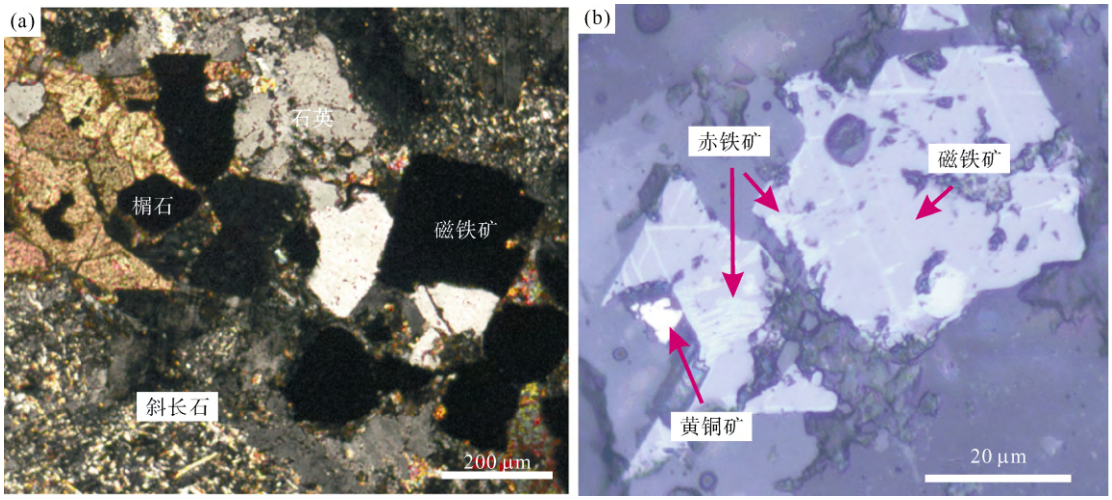

图 7　侏罗纪矿化岩体显微矿物集合体

Fig.7　Mineral assemblages of the mineralized rocks

(a) 卡如花岗岩中榍石-磁铁矿-石英矿物集合体; (b) 卧布闪长斑岩中的磁铁矿-赤铁矿互生, 中间见共生黄铜矿子矿物图。

(a) Quartz-magnetite-titanite assemblage in Karu hornblende granite; (b) magnetite-hematite intergrowth-associated chalcopyrite in Wobu diorite porphyry.

5　矿化岩体的岩浆性质

5.1　高氧化特征

榍石与铁氧化物矿物集合体在一定程度上可反映岩浆氧逸度高低[37]。角闪石+钛铁矿+O_2在合适条件下可形成石英+磁铁矿+榍石(QMT)矿物组合[38], 这说明在更高氧逸度下 QMT 矿物组合比角闪石与钛铁矿组合更稳定。尽管目前并没有直接证据证明 QMT 矿物组合所代表的氧逸度比石英 + 磁铁矿+铁橄榄石(QMF)更高, 但可以确定的是QMT集合体为高氧逸度下的稳定岩浆矿物组合[39–40]。侏罗纪中酸性岩副矿物常见榍石, 其中铜矿化卡如岩体见石英+磁铁矿+榍石矿物组合(图 7a), 表明岩浆具有相对较高的氧逸度。

另外, 岩体中的铁氧化物组合也可反映岩浆氧逸度高低[36,41]。冈底斯南缘侏罗纪侵入岩普遍发育岩浆期磁铁矿, 在矿化岩体如卡如角闪花岗岩、宗噶花岗岩以及卧布闪长斑岩中见赤铁矿-磁铁矿组合(图 7b)。研究表明, 绝大多数斑岩矿床中都发育赤铁矿-磁铁矿矿物组合, 显示岩浆氧逸度甚至达到赤铁矿-磁铁矿(HM)缓冲线, 对斑岩铜矿形成有着重要意义[42]。该矿物组合进一步表明, 冈底斯南缘矿化中酸性岩母岩浆具较高的氧逸度。

5.2　富水及出溶挥发相特征

前人研究表明, 当岩浆中水含量达到 4%时, 可大量析出角闪石[43]。冈底斯南缘早中侏罗世岩浆岩多为富含角闪石的中酸性侵入岩, 这初步表明它们的岩浆可能具有较高的水含量(> 4%)。

富水岩浆在演化早期可能达到水饱和[44], 水饱和的岩浆出溶挥发分相, 会被早期结晶矿物捕获。因此, 较早出溶挥发相的富水岩浆结晶矿物会发育流体包裹体[45–46]。我们在多个矿化岩体的岩浆期结晶矿物, 如自形的榍石、短柱状磷灰石中发现较多气液两相包裹体(图 8)。这类流体包裹在磷灰石或榍石中呈孤立分布, 形状较规则, 显示原生流体包裹体特征。这表明矿化岩体在岩浆富水及在演化较早期达到流体饱和并出溶挥发相。

6　冈底斯南缘早中侏罗世成矿潜力分析

目前在冈底斯南缘发现最古老的弧火山岩侵位于 237~211 Ma[14], 在曲水岩体内出露的角闪辉长岩体侵位于 210 Ma[15], 这些弧岩浆岩的发现表明, 新特提斯洋开始俯冲时间可能不晚于中三叠世。我们在冈底斯南缘发现了多个早中侏罗世的岩浆岩, 结合近年来前人报道的早中生代火山岩和侵入岩[11,14–20,33], 综合表明这些早中侏罗世岩浆岩在冈底斯南缘东西向范围内广泛分布(图 1b), 侵入时代主要集中在 160~190 Ma(图 9 a), 具有弧岩浆的地球化学特征[17,18,20,47]。这表明冈底斯南缘在早-中侏罗世发生了较强烈的岩浆活动, 形成了东西向弧岩浆岩带。

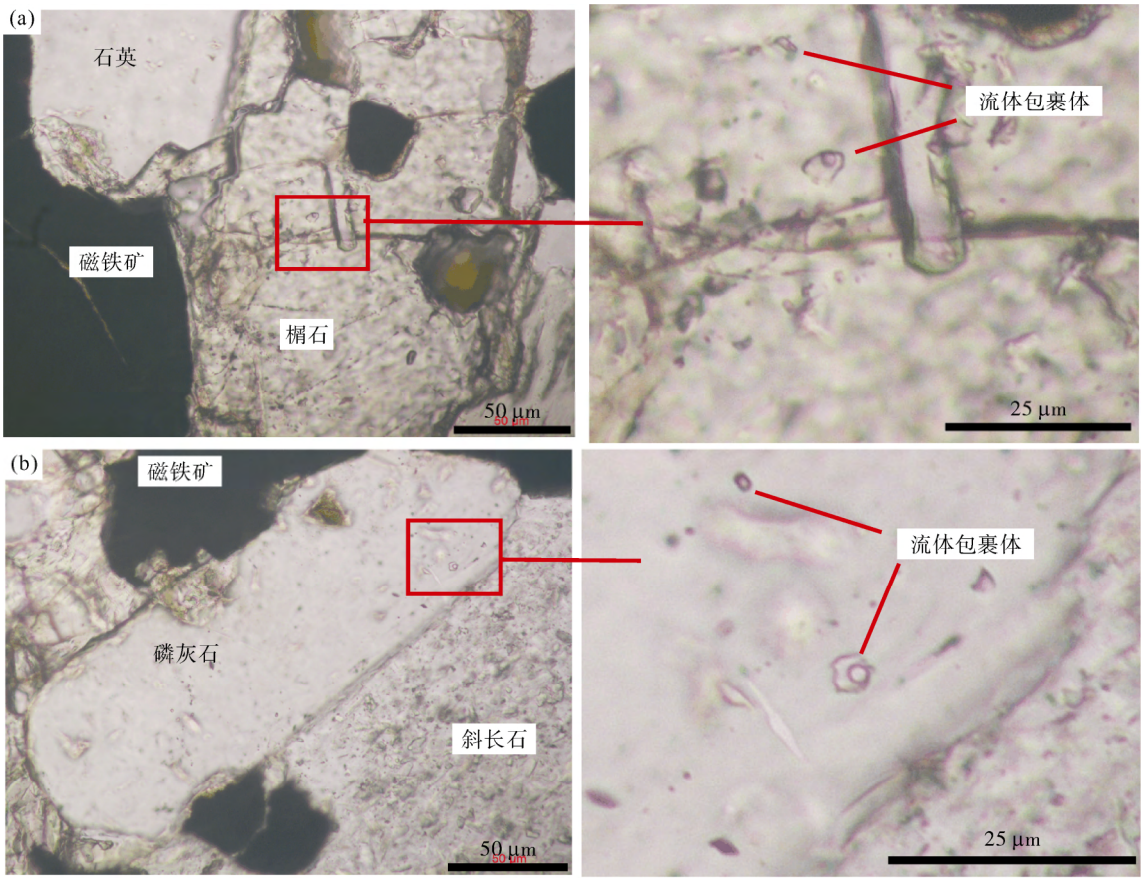

图 8　岩浆早期结晶矿物中的原生流体包裹体

Fig.8　Primary fluid inclusions in the magmatic minerals

(a) 卡如角闪花岗岩，榍石中见气液两相原生流体包裹体; (b) 卧布闪长斑岩，磷灰石中的气液两相原生流体包裹体。

(a) Primary fluid inclusions in the magmatic sphene of Karu hornblende granite; (b) Primary fluid inclusions in the magmatic apatite.

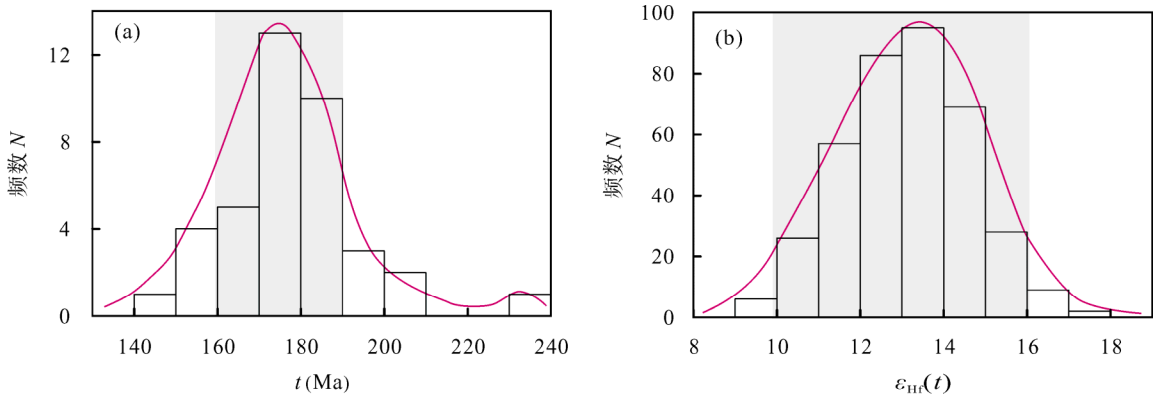

图 9　冈底斯南缘早中生代岩浆岩年龄分布及锆石 Hf 同位素特征(年龄及锆石 Hf 同位素数据引自[11,14–21])

Fig.9　Ages and Hf isotope characteristics of Later Triassic to Jurassic intrusions in South Gangdese (the zircon ages and Hf isotope data are sourced from [11,14–21])

(a) 岩体年龄分布; (b) 锆石$\varepsilon_{Hf}(t)$分布图。

(a) Age distribution; (b) Distribution of zircon $\varepsilon_{Hf}(t)$ values.

目前在这条早中侏罗世弧岩浆带上发现的俯冲型斑岩矿床较少，仅发现有雄村斑岩铜金矿床。有学者认为冈底斯南缘东部侏罗纪弧岩浆作用在下地壳形成硫化物堆积，为碰撞期斑岩矿床提供物质基础[48–49]。我们在西藏谢通门县至尼木县之间的工作发现，冈底斯南缘除雄村之外还发育一系列与侏罗纪岩浆活动有关的铜矿化(图 3)，形成一条约 200 km 与早-中侏罗世岩浆岩有关铜矿化带。因而，冈底斯

南缘在早-中侏罗世发生了较大范围与中酸性岩浆活动有关的成矿作用。

前人研究表明, 斑岩矿床多和中酸性富水高氧逸度岩浆的形成演化有关[36,41,43,44,50–53]。硫在岩浆中主要以氧化硫和还原硫两种形式存在, 氧化硫在岩浆中溶解度较高, 还原硫的溶解度较低[54]。岩浆氧逸度较低时, 硫主要呈还原态, 在岩浆演化早期即达到饱和, 析出硫化物。Cu 在硫化物相和硅酸盐熔体之间的分配系数为 550~10000[55–58], 将大量进入早期结晶析出的硫化物中。因此还原性岩浆不利于 Cu 等成矿元素在岩浆演化过程中富集成矿。Cu、Au 等元素在流体与熔体之间分配系数也很大, Cu 在流体与硅酸盐熔体之间的分配系可达 316~2700[59–60]。富水岩浆较早出溶挥发相, 更有利于成矿元素在挥发相中富集及在岩浆演化晚期成矿[44]。冈底斯南缘多个铜矿化的侵入岩富含角闪石和岩浆期榍石、磷灰石中均发育原生流体包裹体, 显示富水岩浆特征; 同时岩体内发育榍石-磁铁矿-石英以及磁铁矿-赤铁矿共生组合, 显示氧化岩浆特征。上述表明, 冈底斯南缘形成于新特提斯洋俯冲背景的岩体母岩浆具有富水高氧化特征, 有利于亲铜元素在岩浆演化过程中富集成矿。

前人研究表明, MORB 中的 Cu 含量远高于地壳中 Cu 的元素丰度[61], 幔源物质的贡献被认为是金属 Cu 的重要来源。冈底斯带是我国重要的新生代斑岩铜矿带, 相关成矿岩体多具较高锆石 $\varepsilon_{Hf}(t)$值[62], 矿床规模与 $\varepsilon_{Hf}(t)$值有一定的正相关关系[63], 显示亏损地幔或新生地壳源区有利于斑岩矿床的形成。冈底斯南缘早中侏罗世中酸性岩浆岩具较高的 $\varepsilon_{Hf}(t)$值(平均约+13.3), 集中在+10~ +16 之间(图 9 b)[11,14–21], 为有利于形成斑岩型铜矿床的源区。区内雄村超大型斑岩铜金矿床具有较大的锆石 $\varepsilon_{Hf}(t)$值(+10.1~+17.4)[11–12], 也表明冈底斯南缘高 $\varepsilon_{Hf}(t)$值源区有利于形成斑岩铜金矿床。

综上所述, 冈底斯南缘早中侏罗世发育与新特提斯洋壳俯冲有关大规模岩浆活动, 岩浆具高 $\varepsilon_{Hf}(t)$值、富水高氧化及较早出溶挥发相特征, 有利于斑岩铜矿床的形成。另外, 我们已在多个岩体中发现铜矿化相关蚀变, 表明伴随早中侏罗世岩浆活动, 发生了较大范围成矿作用。因此, 冈底斯南缘早中侏罗世与俯冲有关岩浆活动具有良好斑岩矿床成矿潜力。

7　找矿意义

冈底斯南缘目前发育两期俯冲期成矿作用: 分别为以雄村为代表的斑岩铜金矿成矿作用, 与早中侏罗世岩浆活动有关[11]; 以及以克鲁为代表的与矽卡岩型铜金成矿, 与区内大量 90Ma 的岩浆活动有关[64–65]。本文工作表明, 冈底斯南缘早-中侏罗世岩浆活动具有良好的斑岩铜矿成矿潜力, 因此今后应注意在区内寻找与俯冲期岩浆活动有关的斑岩型铜矿床。冈底斯南缘在白垩纪之后经历大规模抬升及强烈的剥蚀, 区内主要出露新生代冈底斯岩基, 大部分早中侏罗世的岩浆岩及相关矿床可能遭受剥蚀。我们在冈底斯南缘多处发现早中侏罗世火山岩及共生侵入岩, 表明冈底斯南缘中生代凹陷地区还保存较完整的早中侏罗世岩浆岩系列。与大面积剥露的冈底斯花岗岩基相比, 桑日群火山岩出露区可能代表剥蚀程度较低的区域。董彦辉等在桑日群中发现了形成于 174 Ma 的中侏罗世火山岩[33], Kang *et al*.也报道了在桑日群火山岩中年龄为 195~189 Ma 的早侏罗世玄武岩[19]。这表明早中侏罗世火山岩分布范围可能比已知区域更为广范。目前的矿产勘查工作已在谢通门县雄村一带早中侏罗世火山岩出露区发现了雄村斑岩型铜金矿床, 本文工作进一步显示谢通门至尼木县之间与侏罗纪俯冲期岩浆活动有关铜矿化带范围长达 200 km。因此, 冈底斯南缘早中侏罗世火山岩出露区应是今后寻找与新特提斯早期俯冲作用有关的斑岩型铜金矿床的主要找矿靶区。

8　结　论

(1) 冈底斯南缘与早-中侏罗世岩浆活动有关铜矿化分布广泛, 形成了东西向与中酸性岩浆活动有关的铜矿化带;

(2) 冈底斯早中侏罗世矿化岩体岩浆具高氧化富水及及较早出溶挥发相特征, 有利于铜在岩浆形成演化过程中富集成矿;

(3) 冈底斯南缘具有良好的俯冲期斑岩铜矿床的成矿潜力, 考虑到冈底斯南缘已发生了大规模剥蚀, 今后找矿靶区应集中在侏罗纪火山岩出露区。

参考文献**(References)**:

[1] Chung S L, Chu M F, Zhang Y Q, Xie Y W, Lo C H, Lee T Y, Lan C Y, Li X H, Zhang Q, Wang Y Z. Tibetan tectonic evolu-

tion inferred from spatial and temporal variations in post-collisional magmatism [J]. Earth Sci Rev, 2005, 68(3/4): 173–196.

[2] Harris N B W, Pearce J A, Tindle A G. Geochemical characteristics of collisionzone magmatism [J]. Geol Soc London Spec Pub, 1986, 19(1): 67–81.

[3] Hou Z Q, Yang Z M, Qu X M, Meng X J, Li Z Q, Beaudoin G, Rui Z Y, Gao Y F, Zaw K. The Miocene Gangdese porphyry copper belt generated during post-collisional extension in the Tibetan Orogen [J]. Ore Geol Rev, 2009, 36(1): 25–51.

[4] Yang Z M, Hou Z Q, White N C, Chang Z S, Li Z Q, Song Y C. Geology of the post-collisional porphyry copper-molybdenum deposit at Qulong, Tibet [J]. Ore Geol Rev, 2009, 36(1/3): 133–159.

[5] 李光明, 芮宗瑶. 西藏冈底斯成矿带斑岩铜矿的成岩成矿年龄[J]. 大地构造与成矿学, 2004, 28(2): 165–170.
Li Guang-ming, Rui Zong-yao. Diagenetic and mineralization ages for the porphyry copper deposits in the Gangdese matallogenic belt, southern Xizang [J]. Geotecton Metallogen, 2004, 28(2): 165–170 (in Chinese with English abstract).

[6] 林武, 梁华英, 张玉泉, 谢应雯. 冈底斯铜矿带冲江含矿斑岩的岩石化学及锆石 SHRIMP 年龄特征[J]. 地球化学, 2004, 33(6): 585–592.
Lin Wu, Liang Hua-ying, Zhang Yu-quan, Xie Ying-wen. Petrochemistry and SHRIMP U-Pb zircon age of the Chongjiang ore-bearing porphyry in the Gangdese porphyry copper belt [J]. Geochimica, 2004, 33(6): 585–592 (in Chinese with English abstract).

[7] 孟祥金, 侯增谦, 高永丰, 黄卫, 曲晓明, 屈文俊. 西藏冈底斯成矿带驱龙铜矿 Re-Os 年龄及成矿学意义[J]. 地质论评, 2003, 49(6): 660–666.
Meng Xiang-jin, Hou Zeng-qian, Gao Yong-feng, Huang Wei, Qu Xiao-ming, Qu Wen-jun. Re-Os dating for molybdenite from Qulong porphyry copper deposit in Gangdese metallogenic belt, Xizang and its metallogenic significance [J]. Geol Rev, 2003, 49(6): 660–666 (in Chinese with English abstract).

[8] 莫济海, 梁华英, 喻亨祥, 陈勇, 孙卫东. 西藏冲木达铜-金(钼)矿床黑云角闪二长花岗岩锆石 U-Pb 年龄及其意义[J]. 地球化学, 2008, 37(3): 206–212.
Mo Ji-hai, Liang Hua-ying, Yu Heng-xiang, Chen Yong, Sun Wei-dong. Zircon U-Pb age of biotite hornblende monzonitic granite for Chongmuda Cu-Au(Mo) deposit in Gangdese belt, Xizang, China and its implications [J]. Geochimica, 2008, 37(3): 206–212 (in Chinese with English abstract).

[9] 曲晓明, 侯增谦, 黄卫. 冈底斯斑岩铜矿(化)带: 西藏第二条“玉龙”铜矿带?[J]. 矿床地质, 2001, 20(4): 355–366.
Qu Xiao-ming, Hou Zeng-qian, Huang Wei. Is Gangdese porphyry copper belt the second “Yulong” copper belt? [J]. Mineral Deposits, 2001, 20(4): 355–366 (in Chinese with English abstract).

[10] 芮宗瑶, 侯增谦, 曲晓明, 张立生, 王龙生, 刘玉琳. 冈底斯斑岩铜矿成矿时代及青藏高原隆升[J]. 矿床地质, 2003, 22(3): 217–225.
Rui Zong-yao, Hou Zeng-qian, Qu Xiao-ming, Zhang Li-sheng, Wang Long-sheng, Liu Yu-lin. Metallogenetic epoch of gangdese porphyry copper belt and uplift of Qinghai-Tibet Plateau [J]. Mineral Deposits, 2003, 22(3): 217–225 (in Chinese with English abstract).

[11] Tafti R, Mortensen J K, Lang J R, Rebagliati M, Oliver J L. Jurassic U-Pb and Re-Os ages for the newly discovered Xietongmen Cu-Au porphyry district, Tibet, PRC: Implications for metallogenic epochs in the southern Gangdese belt [J]. Econ Geol, 2009, 104(1): 127–136.

[12] Tang J X, Lang X H, Xie F W, Gao Y M, Li Z J, Huang Y, Ding F, Yang H H, Zhang L, Wang Q, Zhou Y. Geological characteristics and genesis of the Jurassic No. I porphyry Cu-Au deposit in the Xiongcun district, Gangdese porphyry copper belt, Tibet [J]. Ore Geol Rev, 2015, 70(4): 438–456.

[13] 邹银桥, 黄文婷, 梁华英, 伍静, 林书平, 王秀璋. 西藏冈底斯南缘雄村铜金矿床成矿斑岩厘定及其锆石 U-Pb 和黑云母 Ar-Ar 年龄分析[J]. 岩石学报, 2015, 31(7): 2053–2062.
Zou Yin-qiao, Huang Wen-ting, Liang Hua-ying, Wu Jing, Lin Shu-ping, Wang Xiu-zhang. Identification of porphyry genetically associated with mineralization and its zircon U-Pb and biotite Ar-Ar age of the Xiongcun Cu-Au deposit, southern Gangdese, Tibet [J]. Acta Petrol Sinica, 2015, 31(7): 2053–2062 (in Chinese with English abstract).

[14] Wang C, Ding L, Zhang L Y, Kapp P, Pullen A, Yue Y H. Petrogenesis of Middle-Late Triassic volcanic rocks from the Gangdese belt, southern Lhasa terrane: Implications for early subduction of Neo-Tethyan oceanic lithosphere [J]. Lithos, 2016, 262: 320–333.

[15] Meng Y K, Xu Z Q, Santosh M, Ma X X, Chen X J, Guo G L, Liu F. Late Triassic crustal growth in southern Tibet: Evidence from the Gangdese magmatic belt [J]. Gondw Res, 2015, 37: 449–464.

[16] Chu M F, Chung S L, Song B, Liu D Y, O’Reilly S Y, Pearson Norman J, Ji J Q, Wen D J. Zircon U-Pb and Hf isotope constraints on the Mesozoic tectonics and crustal evolution of southern Tibet [J]. Geology, 2006, 34(9): 745–748.

[17] Guo L S, Liu Y L, Liu S W, Cawood Peter A, Wang Z H, Liu H F. Petrogenesis of Early to Middle Jurassic granitoid rocks from the Gangdese belt, Southern Tibet: Implications for early history of the Neo-Tethys [J]. Lithos, 2013, 179(5): 320–333.

[18] Ji W Q, Wu F Y, Chung S L, Li J X, Liu C Z. Zircon U-Pb geochronology and Hf isotopic constraints on petrogenesis of the Gangdese batholith, southern Tibet [J]. Chem Geol, 2009, 262(3/4): 229–245.

[19] Kang Z Q, Xu J F, Wilde S A, Feng Z H, Chen J L, Wang B D, Fu W C, Pan H B. Geochronology and geochemistry of the Sangri Group Volcanic Rocks, Southern Lhasa Terrane: Implications for the early subduction history of the Neo-Tethys and Gangdese Magmatic Arc [J]. Lithos, 2014, 200–201: 157–168.

[20] 张宏飞, 徐旺春, 郭建秋, 宗克清, 蔡宏明, 袁洪林. 冈底斯南缘变形花岗岩锆石 U-Pb 年龄和 Hf 同位素组成: 新特提斯洋早侏罗世俯冲作用的证据[J]. 岩石学报, 2007, 23(6): 1347–1353.

Zhang Hong-fei, Xu Wang-chun, Guo Jian-qiu, Zong Ke-qing, Cai Hong-ming, Yuan Hong-lin. Zircon U-Pb isotopic composition of deformed granite in the southern margin of the Gangdese belt, Tibet: Evidence for early Jurassic subduction of Neo-Tethyan oceanic slab [J]. Acta Petrol Sinica, 2007, 23(6): 1347–1353 (in Chinese with English abstract).

[21] Liu C Z, Chung S L, Wu F Y, Zhang C, Xu Y, Wang J G, Chen Y, Guo S. Tethyan suturing in Southeast Asia: Zircon U-Pb and Hf-O isotopic constraints from Myanmar ophiolites [J]. Geology, 2016, 44(4): 311–314.

[22] Searle M P, Windley B F, Coward M P, Cooper D J W, Rex A J, Rex D, Li T D, Xiao X C, Jan M Q, Thakur V C, Kumar S. The closing of Tethys and the tectonics of the Himalaya [J]. Geol Soc Am Bull, 1987, 98(6): 678–701.

[23] 潘桂棠, 莫宣学, 侯增谦, 朱弟成, 王立全, 李光明, 赵志丹, 耿全如, 廖忠礼. 冈底斯造山带的时空结构及演化[J]. 岩石学报, 2006, 22(3): 521–533.
Pan Gui-tang, Mo Xuan-xue, Hou Zeng-qian, Zhu Di-chegn, Wang Li-quan, Li Guang-ming, Zhao Zhi-dan, Gong Quan-ru, Liao Zhong-li. Spatial-temporal framework of the Gangdese orogenic belt and itsevokution [J]. Acta Petrol Sinica, 2006, 22(3): 521–533 (in Chinese with English abstract).

[24] Chiu H Y, Chung S L, Wu F Y, Liu D Y, Liang Y H, Lin I J, Iizuka Y, Xie L W, Wang Y B, Chu M F. Zircon U-Pb and Hf isotopic constraints from eastern Transhimalayan batholiths on the precollisional magmatic and tectonic evolution in southern Tibet [J]. Tectonophysics, 2009, 477(1/2): 3–19.

[25] Chung S L, Chu M F, Ji J Q, O'Reilly S Y, Pearson N J, Liu D Y, Lee T Y, Lo C H. The nature and timing of crustal thickening in Southern Tibet: Geochemical and zircon Hf isotopic constraints from postcollisional adakites [J]. Tectonophysics, 2009, 477(1/2): 36–48.

[26] 莫宣学, 董国臣, 赵志丹, 周肃, 王亮亮, 邱瑞照, 张风琴. 西藏冈底斯带花岗岩的时空分布特征及地壳生长演化信息[J]. 高校地质学报, 2005, 11(3): 281–290.
Mo Xuan-xue, Dong Guo-chen, Zhao Zhi-dan, Zhou Su, Wang Liang-liang, Qiu Rui-zhao, Zhang Feng-qin. Spatial and temporal distribution and characteristics of granitoids in the Gangdese Tibet and implication for crustal growth and evolution [J]. Geol J China Univ, 2005, 11(3): 281–290 (in Chinese with English abstract).

[27] Mo X X, Hou Z Q, Niu Y L, Dong G C, Qu X M, Zhao Z D, Yang Z M. Mantle contributions to crustal thickening during continental collision: Evidence from Cenozoic igneous rocks in southern Tibet [J]. Lithos, 2007, 96(1/2): 225–242.

[28] Ma L, Wang Q, Wyman D A, Li Z X, Jiang Z Q, Yang J H, Gou G N, Guo H F. Late Cretaceous (100–89 Ma) magnesian charnockites with adakitic affinities in the Milin area, eastern Gangdese: Partial melting of subducted oceanic crust and implications for crustal growth in southern Tibet [J]. Lithos, 2013, 175–176: 315–332.

[29] Zhu D C, Mo X X, Wang L Q, Zhao Z D, Niu Y L, Zhou C Y, Yang Y H. Petrogenesis of highly fractionated I-type granites in the Zayu area of eastern Gangdese, Tibet: Constraints from zircon U-Pb geochronology, geochemistry and Sr-Nd-Hf isotopes [J]. Sci China (D), 2009, 52(9): 1223–1239.

[30] Ji W Q, Wu F Y, Chung S L, Liu C Z. The Gangdese magmatic constraints on a latest Cretaceous lithospheric delamination of the Lhasa terrane, southern Tibet [J]. Lithos, 2014, 210–211: 168–180.

[31] Wen D R, Liu D Y, Chung S L, Chu M F, Ji J Q, Zhang Q, Song B, Lee T Y, Yeh M W, Lo C H. Zircon SHRIMP U-Pb ages of the Gangdese Batholith and implications for Neotethyan subduction in southern Tibet [J]. Chem Geol, 2008, 252(3/4): 191–201.

[32] Wen D R, Chung S L, Song B, Iizuka Y, Yang H J, Ji J Q, Liu D Y, Gallet S. Late Cretaceous Gangdese intrusions of adakitic geochemical characteristics, SE Tibet: Petrogenesis and tectonic implications [J]. Lithos, 2008, 105(1/2): 1–11.

[33] 董彦辉, 许继峰, 曾庆高, 王强, 毛国政, 李杰. 存在比桑日群弧火山岩更早的新特提斯洋俯冲记录么? [J]. 岩石学报, 2006, 22(3): 661–668.
Dong Yan-hui, Xu Ji-feng, Zeng Qing-gao, Wang Qiang, Mao Guo-zheng, Li Jie. Is there a Neo-Tethys' subduction record earlier than arc volcanic rocks in the Sangri Group? [J]. Acta Petrol Sinica, 2006, 22(3): 661–668 (in Chinese with English abstract).

[34] Zhu D C, Pan G T, Chung S L, Liao Z L, Wang L Q, Li G M. SHRIMP zircon age and geochemical constraints on the origin of lower Jurassic volcanic rocks from the Yeba formation, Southern Gangdese, south Tibet [J]. Int Geol Rev, 2008, 50(5): 442–471.

[35] Zhu D C, Zhao Z D, Niu Y L, Dilek Y, Hou Z Q, Mo X X. The origin and pre-Cenozoic evolution of the Tibetan Plateau [J]. Gondw Res, 2013, 23(4): 1429–1454.

[36] Sun W D, Liang H Y, Ling M X, Zhan M Z, Ding X, Zhang H, Yang X Y, Li Y L, Ireland T R, Wei Q R, Fan W M. The link between reduced porphyry copper deposits and oxidized magmas [J]. Geochim Cosmochim Acta, 2013, 103(2): 263–275.

[37] Wones D R. Significance of the Assemblage Titanite + Magnetite + Quartz in Granitic-Rocks [J]. Am Mineral, 1989, 74(7): 744–749.

[38] Harlov D, Tropper P, Seifert W, Nijland T, Forster H J. Formation of Al-rich titanite ($CaTiSiO_4O$-$CaAlSiO_4OH$) reaction rims on ilmenite in metamorphic rocks as a function of f_{H2O} and f_{O2} [J]. Lithos, 2006, 88(1): 72–84.

[39] Xirouchakis D, Lindsley D H. Assemblages with titanite ($CaTiOSiO_4$), Ca-Mg-Fe olivine and pyroxenes, Fe-Mg-Ti oxides, and quartz: Part I. Theory [J]. Am Mineral, 2001, 86(3): 247–253.

[40] Xirouchakis D, Lindsley D H. Assemblages with titanite ($CaTiOSiO_4$), Ca-Mg-Fe olivine and pyroxenes, Fe-Mg-Ti oxides, and quartz: Part II. Application [J]. Am Mineral, 2001, 86(3): 254–264.

[41] Liang H Y, Sun W D, Su W C, Zartman R E. Porphyry copper-gold mineralization at Yulong, China, promoted by decreasing redox potential during magnetite alteration [J]. Econ

Geol, 2009, 104(4): 587–596.

[42] Sun W D, Huang R F, Li H, Hu Y B, Zhang C C, Sun S J, Zhang L P, Ding X, Li C Y, Zartman R E, Ling M X. Porphyry deposits and oxidized magmas [J]. Ore Geol Rev, 2015, 65: 97–131.

[43] Kelley K A, Cottrell E. Water and the oxidation state of subduction zone magmas [J]. Science, 2009, 325(5940): 605–607.

[44] Richards J P. High Sr/Y arc magmas and porphyry Cu^{+}-Mo^{+}-Au deposits: Just add water [J]. Econ Geol, 2011, 106(7): 1075–1081.

[45] Huang W T, Wu J, Zhang J, Liang H Y, Qiu X N. Geochemistry and Hf-Nd isotope characteristics and forming processes of the Yuntoujie granites associated with W-Mo deposit, Guangxi, South China [J]. Ore Geol Rev, 2016, 81(2): 953–964.

[46] 伍静, 梁华英, 黄文婷, 王春龙, 孙卫东, 孙亚莉, 李晶, 莫济海, 王秀璋. 桂东北苗儿山-越城岭南西部岩体和矿床同位素年龄及华南印支期成矿分析 [J]. 科学通报, 2012, 57(13): 1126–1136.
Wu Jing, Liang Huaying, Huang Wenting, Wang Chunlong, Sun Weidong, Sun Yali, Li Jing, Mo Jihai, Wang Xiuzhang. Identification of coesite-bearing amphibolite in the North Qinling and its geological significance [J]. Chinese Sci Bull, 2012, 57(13): 1126–1136 (in Chinese).

[47] Ji W Q, Wu F Y, Liu C Z, Chung S L. Geochronology and petrogenesis of granitic rocks in Gangdese batholith, southern Tibet [J]. Sci China (D), 2009, 52(9): 1240–1261.

[48] Hou Z Q, Yang Z M, Lu Y J, Anthony K, Zheng Y C, Li Q Y, Tang J X, Yang Z S, Duan L F. A genetic linkage between subduction- and collision-related porphyry Cu deposits in continental collision zones [J]. Geology, 2015, 43(3): 247–250.

[49] Wang R, Reza T, Hou Z Q, Shen Z C, Guo N, Noreen E J, Heejin J, Li Q Y, Li W K. Across-arc geochemical variation in the Jurassic magmatic zone, Southern Tibet: Implication for continental arc-related porphyry Cu-Au mineralization [J]. Chem Geol, 2017, 451: 116–134.

[50] Cline J S. How to concentrate copper [J]. Science, 2003, 302(5653): 2075–2076.

[51] Liang H Y, Campbell I H, Allen C, Sun W D, Liu C Q, Yu H X, Xie Y W, Zhang Y Q. Zircon Ce^{4+}/Ce^{3+} ratios and ages for Yulong ore-bearing porphyries in eastern Tibet [J]. Mineral Deposita, 2006, 41(2): 152–159.

[52] Mungall J E. Roasting the mantle: Slab melting and the genesis of major Au and Au-rich Cu deposits [J]. Geology, 2002, 30(10): 915–918.

[53] Sillitoe R H. Porphyry Copper Systems [J]. Econ Geol, 2010, 105(1): 3–41.

[54] Mungall J E, Hanley J J, Arndt N T, Debecdelievre A. Evidence from meimechites and other lowdegree mantle melts for redox controls on mantle-crust fractionation of platinum group elements [J]. Proc Natl Acad Sci USA, 2006, 103(34): 12695–12700.

[55] Gaetani G A, Grove T L. Partitioning of moderately siderophile elements among olivine, silicate melt, and sulfide melt: Constraints on core formation in the Earth and Mars [J]. Geochim Cosmochim Acta, 1997, 61(9): 1829–1846.

[56] Halter W E, Pettke T, Heinrich C A. The origin of Cu/Au ratios in porphyry-type ore deposits [J]. Science, 2002, 296(5574): 1844–1846.

[57] Jugo P J, Candela P A, Piccoli P M. Magmatic sulfides and Au: Cu ratios in porphyry deposits: An experimental study of copper and gold partitioning at 850 °C, 100 MPa in a haplogranitic melt-pyrrhotite-intermediate solid solution-gold metal assemblage, at gas saturation [J]. Lithos, 1999, 46(3): 573–589.

[58] Keppler H, Wyllie P J. Partitioning of Cu, Sn, Mo, W, U, and Th between melt and aqueous fluid in the systems haplogranite-H_2O-HCl and haplogranite-H_2O-HF [J]. Contrib Mineral Petrol, 1991, 109(2): 139–150.

[59] Simon A C, Pettke T, Candela P A, Piccoli P M, Heinrich C A. Copper partitioning in a melt-vapor-brine-magnetite- pyrrhotite assemblage [J]. Geochim Cosmochim Acta, 2006, 70(22): 5583–5600.

[60] Zajacz Z, Halter W E, Pettke T, Guillong M. Determination of fluid/melt partition coefficients by LA-ICPMS analysis of co-existing fluid and silicate melt inclusions: Controls on element partitioning [J]. Geochim Cosmochim Acta, 2008, 72(8): 2169–2197.

[61] Hofmann A W. Chemical differentiation of the Earth: The relationship between mantle, continental crust, and oceanic crust [J]. Earth Planet Sci Lett, 1988, 90(3): 297–314.

[62] Hou Z Q, Zheng Y C, Yang Z M, Rui Z Y, Zhao Z D, Jiang S H, Qu X M, Sun Q Z. Contribution of mantle components within juvenile lower-crust to collisional zone porphyry Cu systems in Tibet [J]. Mineral Deposita, 2012, 48(2): 173–192.

[63] 侯增谦, 杨志明. 中国大陆环境斑岩型矿床: 基本地质特征、岩浆热液系统和成矿概念模型[J]. 地质学报, 2009, 83(12): 1779–1817.
Hou Zeng-qian, Yang Zhi-ming. Porphyry deposits in continental settings of China: Geological characteristics, magmatic-hydrothermal system, and metallogenic model [J]. Acta Geol Sinica, 2009, 83(12): 1779–1817 (in Chinese with English abstract).

[64] 梁华英, 魏启荣, 许继峰, 胡光黔. 西藏冈底斯矿带南缘矽卡岩型铜矿床含矿岩体锆石 U-Pb 年龄及意义[J]. 岩石学报, 2010, 26(6): 1693–1698.
Liang Hua-ying, Wei Qi-rong, Xu Ji-feng, Hu Guang-qian. Study on zircon LA-ICP-MS U-Pb age of skarn Cu mineralization related intrusion in the southern margin of the Gangdese ore belt, Tibet and its geological implication [J]. Acta Petrol Sinica, 2010, 26(6): 1692–1698 (in Chinese with English abstract).

[65] Chen L, Qin K Z, Li G M, Li J X, Xiao B, Zhao J X, Fan X. Zircon U-Pb ages, geochemistry, and Sr-Nd-Pb-Hf isotopes of the Nuri intrusive rocks in the Gangdese area, southern Tibet: Constraints on timing, petrogenesis, and tectonic transformation [J]. Lithos, 2015, 212–215: 379–396.